



LAWRENCE
LIVERMORE
NATIONAL
LABORATORY

Optimized Non-Orthogonal Localized Orbitals for Electronic Structure Calculations: Improved Linear Scaling Quantum Monte Carlo

F. A. Reboredo, A. J. Williamson

July 28, 2004

Physical Review B

Disclaimer

This document was prepared as an account of work sponsored by an agency of the United States Government. Neither the United States Government nor the University of California nor any of their employees, makes any warranty, express or implied, or assumes any legal liability or responsibility for the accuracy, completeness, or usefulness of any information, apparatus, product, or process disclosed, or represents that its use would not infringe privately owned rights. Reference herein to any specific commercial product, process, or service by trade name, trademark, manufacturer, or otherwise, does not necessarily constitute or imply its endorsement, recommendation, or favoring by the United States Government or the University of California. The views and opinions of authors expressed herein do not necessarily state or reflect those of the United States Government or the University of California, and shall not be used for advertising or product endorsement purposes.

Optimized Non-Orthogonal Localized Orbitals for Electronic Structure Calculations: Improved Linear Scaling Quantum Monte Carlo

Fernando A. Reboredo* and Andrew J. Williamson†
Lawrence Livermore National Laboratory, Livermore, CA 94550

We derive an automatic procedure for generating a set of highly localized, non-orthogonal orbitals for linear scaling quantum Monte Carlo calculations. We demonstrate the advantage of these orbitals in calculations of the total energy of both semiconducting and metallic systems by studying bulk silicon and the homogeneous electron gas. For silicon, the improved localization of these orbitals reduces the computational time by a factor five and the memory by a factor of six compared to localized, orthogonal orbitals. For jellium, we demonstrate that the total energy is converged for orbitals truncated within spheres with radii 7-8 r_s , opening the possibility of linear scaling QMC calculations for realistic metallic systems.

In recent years, one of the most promising developments in the field of electronic structure calculations has been the development of algorithms whose cost grows as the first power of the system size. Linear scaling variants of several electronic structure techniques have been developed, including tight-binding[1], density functional theory (DFT)[1–6], coupled cluster[7] and quantum Monte Carlo (QMC)[8, 9]. In all these approaches extended Bloch orbitals, ψ_{nk} , are transformed into localized Wannier-like orbitals. The speedup provided by the transformation to localized orbitals depends on the extent to which the orbitals can be localized and subsequently truncated. Therefore, improved methods for constructing localized orbitals have attracted intense attention in recent years[10–12]. Of particular relevance to this paper is the recent demonstration that generalizing from conventional orthonormal Wannier orbitals to non-orthogonal orbitals[1–6] can provide increased localization and further accelerate linear scaling DFT algorithms.

In QMC calculations, truncated, localized orbitals can be used to introduce sparsity into the Slater determinant part of the trial wave function. As the calculation of the orbitals used to construct this determinant is the dominant cost of QMC calculations, this transformation yields a near linear scaling QMC algorithm. In our original approach to linear scaling QMC calculations[8], the Slater determinant was constructed from a set of orthonormal Wannier functions. This choice of orbitals produces a near linear scaling algorithm, which has successfully been applied to calculations of the total energies and optical gaps of a variety of semiconductor systems[13, 14]. However, this method suffers from three main limitations: (i) It is only applicable to systems where the Wannier functions decay rapidly (exponentially), i.e., it works well for semiconductors and insulators, but it is not applicable to metallic systems where orthonormal Wannier functions decay polynomially[11]. (ii) The Wannier functions are constructed via a unitary transformation of an input set of Bloch functions. This limits one to orthogonal functions, while a non-zero Slater determinant requires only

that the orbitals are linearly independent. (iii) Truncating a localized function reduces the volume in which it needs to be evaluated, speeding up the calculation. However, the Metropolis algorithm samples configurations of electron coordinates from the many-body wavefunction, hence, some points are sampled more frequently than others. This knowledge of the wavefunction is not included in the generation of the orthonormal orbitals and hence the choice of orbitals is not optimal.

In this letter we derive and demonstrate the use of a *non-orthogonal* transformation of the Bloch orbitals that overcomes the above limitations. This transformation is based on algorithms developed for linear scaling DFT calculations[1–6] and is designed to minimize a cost function associated with the total number of orbital evaluations required in a linear scaling QMC calculation. For representative semiconductor systems, the orbitals obtained from this non-orthogonal transformation are significantly more localized and smoother than orthogonal Wannier functions, and can typically be truncated in one sixth of the volume of the equivalent orthogonal function without sacrificing accuracy. This produces an algorithm ~ 5 times faster than previous linear scaling QMC calculations[8] and requiring one sixth of the memory. In addition, we demonstrate that while orthogonal Wannier functions for metallic systems cannot be truncated within a practical volume, non-orthogonal orbitals constructed via our procedure can be truncated within a practical cutoff radius.

Our QMC calculations use a linear scaling[8] version of the CASINO[15] code with a standard Slater-Jastrow trial wavefunction, $\Psi_T(\mathbf{R})$ [16]. The Slater determinants are constructed from a set of truncated, localized linearly independent orbitals $D_{ij} = \phi_i(\mathbf{r}_j)\Theta_i(\mathbf{r}_j)$, where ϕ are the non-orthogonal orbitals and Θ are the truncation functions. In principle, one can optimize the shape of the truncation functions, however, for the systems studied here, we find that spherical step functions are a simple and stable solution where,

$$\begin{aligned} \Theta^i(\mathbf{r}) &= 1, & |\mathbf{r} - \mathbf{R}_i| < R_i^{cut} \\ &= 0, & |\mathbf{r} - \mathbf{R}_i| > R_i^{cut} \end{aligned} \quad (1)$$

The truncation functions Θ^i are defined by two parameters, the cutoff radii R_i^{cut} and the centers \mathbf{R}_i . These parameters are optimized iteratively using a procedure designed to minimize the computational cost of the QMC calculation. The non-orthogonal orbitals, ϕ_i , associated with each Θ^i are obtained during the iterative process.

The computational cost of a typical QMC calculation is proportional to the number of orbital evaluations required to construct the Slater determinant for each configuration of electron coordinates, $\mathbf{R} = (\mathbf{r}_1, \mathbf{r}_2 \dots \mathbf{r}_N)$. The cost is therefore the product of the probability, $|\Psi_T(\mathbf{R})|^2$, of sampling a given configuration, \mathbf{R} and the cost of evaluating each of the non-zero elements in the Slater determinant produced by that configuration. For each element, $\phi_i(\mathbf{r}_j)$, if \mathbf{r}_j falls within the truncation function, Θ_i , this adds 1 to the cost, i.e.

$$\text{Cost} = \int d\mathbf{R} |\Psi_T(\mathbf{R})|^2 \sum_{ij}^N \Theta_i(\mathbf{r}_j) . \quad (2)$$

By integrating out all but one electron coordinates, Eq.(2) can be expressed in terms of the density $\rho(\mathbf{r})$ as

$$\text{Cost} = \sum_i \int d\mathbf{r} \rho(\mathbf{r}) \Theta_i(\mathbf{r}) . \quad (3)$$

We find a satisfactory minimum of Eq. (3) by starting from an initial choice of Θ_i and iteratively updating first the cutoff radii R_i^{cut} and then the centers \mathbf{R}_i .

(i) *Generating Optimal Non-Orthogonal Orbitals and Cutoff Radii:* Each truncation function, Θ_i , can be considered as a potential, \hat{V} , acting on the Hilbert space of Bloch orbitals. In the inset to Fig 1a this potential, \hat{V} , is shown with a blue line. If one constructs the matrix elements of the Bloch orbitals with this potential, $V_{jk}^i = \langle \phi_j^{Bloch} | \Theta^i(\mathbf{r}) | \phi_k^{Bloch} \rangle$, then the eigenstate ϕ_i of V^i with the largest eigenvalue is the most localized state within the truncation region. This is the orbital with the maximum truncated norm, X , defined as

$$X = \int d\mathbf{r} |\phi_i(\mathbf{r})|^2 \Theta_i(\mathbf{r}) . \quad (4)$$

Increasing R_i^{cut} increases the above value of X , reducing the resulting truncation error in the QMC calculation, but also increases the computational cost in Eq.(3). Therefore, we adjust the cutoff radius R_i^{cut} to achieve a target norm, e.g. $X = 0.999$. Repeating this diagonalization procedure for each truncation function Θ^i generates an associated set of non-orthogonal orbitals $\{\phi\}$. This procedure for generating a set of non-orthogonal orbitals associated with a set of truncation regions is similar to those adopted in linear scaling density functional calculations[1, 3, 4, 6] and recently in a QMC calculation of MgO[9]. Next, we extend this procedure to automatically optimize the centers of the truncation functions for systems where they cannot be guessed *a priori*.

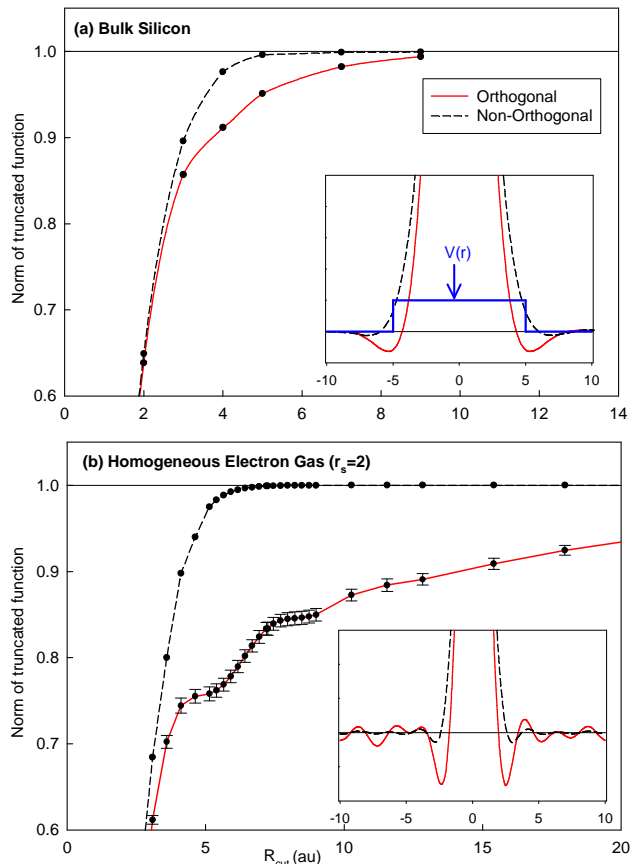


FIG. 1: (Color) Comparison of the norm of orthogonal and non-orthogonal localized orbitals in (a) bulk silicon and (b) a HEG at the same r_s . The error bars show the spread in norm between the states. The insets compare the shape of the orthogonal and non-orthogonal localized orbitals.

(ii) *Updating the Truncation Centers:* The cost function in Eq. (3) can be rewritten as

$$\text{Cost} = NX + \sum_i \int d\mathbf{r} [\rho(\mathbf{r}) - |\phi_i(\mathbf{r})|^2] \Theta_i(\mathbf{r}) , \quad (5)$$

where N is the number of orbitals and X is defined in Eq.(4). The first term in Eq.(5), NX , cannot be reduced without losing accuracy. Therefore the only way to reduce the computational cost is to minimize the second term in Eq.(5) by placing the truncation centers where $\rho(\mathbf{r}) - |\phi_i(\mathbf{r})|^2$ is minimum. Since $\rho(\mathbf{r}) \geq |\phi_i(\mathbf{r})|^2$, this is minimized in regions where ϕ_i is most localized and therefore closest to ρ . Therefore for the next iteration, we move the truncation centers towards the center of mass of the $|\phi_i(\mathbf{r})|^2$ for the current iteration. To ensure linear independence, we orthogonalize the set $\{\phi\}$ with a polar decomposition before calculating this center of mass.

This updated set of truncation functions, Θ^i , with new centers, \mathbf{R}_i , are then used to generate a new set of non-orthogonal orbitals using the procedure in (i) above and

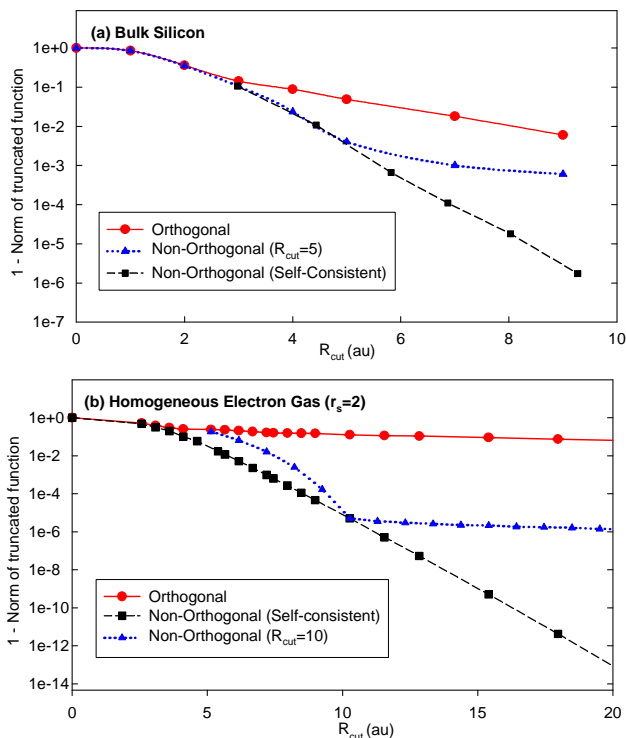


FIG. 2: (Color) Comparison of the decay of orthogonal, self consistent, non-orthogonal and fixed radius, non-orthogonal localized orbitals in (a) bulk silicon and (b) HEG ($r_s = 2$).

the process is repeated. Starting from a random choice of centers 10-15 iterations are typically required to find a minimum of Eq. (3) and to converge the centers. If one uses a good starting set of centers, such as the centers of maximally localized Wannier functions[10], the Θ_i converge in 1 or 2 iterations.

To analyze the properties of these new non-orthogonal orbitals we first compare their localization and decay properties with an equivalent set of orthogonal orbitals. We then examine the convergence of the total energy in quantum Monte Carlo calculations using these orbitals. Comparisons are made for the prototypical semiconductor and metal systems, silicon and the homogeneous electron gas.

In Fig. 1 the norm within a spherical truncation region of the orthogonal and non-orthogonal localized orbitals are compared as a function of R_{cut} . Fig. 1(a) compares orbitals constructed for bulk silicon. The input states were obtained from a 64 atom LDA calculation[18], using a norm-conserving Hamann pseudopotential and a 35 Ry cutoff. The non-orthogonal orbitals were constructed using the iterative procedure described above, where the desired norm, X , was varied from 0.5 to 0.99999 to construct the plot. The orthogonal states were obtained by performing a final polar decomposition orthogonalization step. Due to symmetry all the non-orthogonal orbitals are equivalent. Within a given radius, the non-

orthogonal orbitals contain significantly more charge, e.g. 99.9% of the norm is contained within a sphere of radius 5.5 au compared to orthogonal orbitals which require an 11 au sphere to capture the same charge. The origin of this dramatically improved localization is shown in the inset to Fig. 1(a) which shows a line plot through the center of the $R_{cut} = 2$ orbitals. While the non-orthogonal states decay smoothly to zero with minimal oscillations, the orthogonal orbitals oscillate around zero for > 5 au after initially crossing zero to maintain orthogonality between states. While the amplitude of these oscillations is small compared to the central peak, the r^2 prefactor leaves a significant amount of charge in these oscillations.

Comparing the orthogonal orbitals shown in Fig. 1(a) with maximally localized (MLW) orbitals constructed according to Ref.[10], which essentially finds the localized eigenstates of the $e^{i2\pi\mathbf{r}/L}$ operator, we find the centers of our non-orthogonal and orthogonal states are identical to the MLW function centers due to symmetry. Additionally, the shape and norm convergence of our orthogonal states is almost identical to the MLW functions. It therefore appears that the shape of *orthogonal* localized orbitals is relatively insensitive to the choice of operator used to localize the states.

Figure 1(b) shows orthogonal and non-orthogonal orbitals constructed for the HEG with $r_s = 2$ (same as silicon). The input states were the lowest 1935 plane waves in a 50 au cubic box. The norm of the orthogonal orbitals slowly approaches 1.0 as the radius is increased, as would be expected given the slow polynomial decay of orthogonal orbitals in metallic systems[11]. In contrast, the non-orthogonal orbitals rapidly approach 1. For example 99.9% of the norm of the non-orthogonal orbitals is contained within a sphere of radius 7 au, while even the largest sphere inscribed within the supercell (25 au radius) contains only 94% of the norm of the orthogonal orbitals. Note, the non-orthogonal orbitals are still less localized than those in silicon, where 99.9% of the norm is contained within a sphere of radius 5.5 au compared to the 7 au required for jellium. As in silicon, the inset plot shows pronounced, long range oscillations in the orthogonal orbitals and a much smoother decay of the non-orthogonal orbitals with minimal oscillation.

Figure 2 compares the truncated decay of orthogonal and non-orthogonal localized orbitals for bulk silicon and the HEG. This is equivalent to the decay of the trace of the non-orthogonal density matrix[1, 2, 5]. Here we define the decay as 1 minus the norm contained within a sphere of radius R . As expected from Fig. 1, Fig. 2 shows that the non-orthogonal orbitals (black dashed lines) decay more rapidly than the equivalent orthogonal orbitals (red solid lines). Figure 2 also illustrates that to obtain maximum localization within a given volume, the non-orthogonal orbitals must be adjusted consistently with R_{cut} [17]. The blue dotted line in Fig.2b shows the decay of a non-orthogonal orbital optimized to be maximally

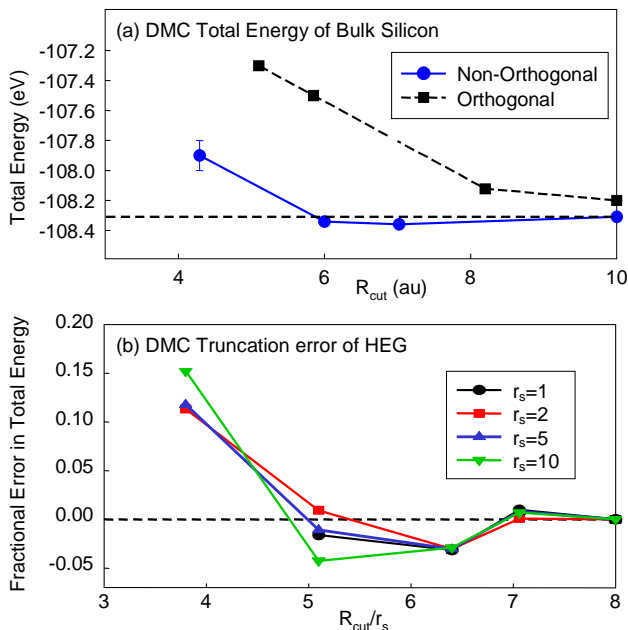


FIG. 3: (Color) (a) Convergence of DMC total energy of bulk silicon with truncation radius for orthogonal and non-orthogonal orbitals, (b) Convergence of DMC total energy of the HEG as a function of R_{cut}/r_s

localized in a Θ function with $R_{cut} = 10$. The truncated norm was then evaluated for a range of R values while keeping the orbital fixed. For $R_{cut} = 10$ the “self-consistent” and fixed non-orthogonal orbitals are identical. For all other values of R_{cut} , the orbital optimized with $R_{cut} = 10$ (blue,dotted) is no longer the optimal orbital for that choice of Θ function and it therefore has a lower truncated norm.

Our previous work with orthogonal, truncated, localized orbitals[8] indicated that the norm of these orbitals was a good predictor of the truncation error in a QMC calculation the total energy. For silicon we found that a truncation region large enough to capture 99.9% of the norm was sufficient to produce a converged total energy. On this basis, the improved decay properties of the non-orthogonal orbitals shown in Figs. 1 and 2 suggest that these orbitals can be used to perform QMC calculations with smaller truncation radii than those used for previous orthogonal orbitals, without sacrificing accuracy. However, the decay of the localized orbitals in a given representation does not predict the truncation error in the density matrix and how electron-electron correlation will be affected. Therefore, to fully evaluate the properties of these non-orthogonal orbitals we have performed VMC and DMC total energy calculations of bulk silicon and the HEG to compare the convergence of the total energy with the truncation radii of the localized orbitals.

Figure 3(a) compares the convergence of the DMC total energy of the same 64 atom, bulk silicon system shown in Figs. 1(a) and Fig. 2 (a), using orthogonal and non-

orthogonal input orbitals. It shows that the DMC energy converges more rapidly using non-orthogonal orbitals. To converge the total energy to within 0.01 eV per atom using orthogonal orbitals required $R_{cut} = 11$ au[8] while using non-orthogonal orbitals, equivalent accuracy can be obtained with $R_{cut} = 6$ au. This results in a factor of 5 increase in speed and a factor of 6 reduction in memory.

Figure 3(b) compares the convergence with R_{cut} of the DMC total energy of a homogeneous electron gas with $r_s = 1, 2, 5$ and 10. In the HEG, the non-orthogonal orbitals for all r_s values can be obtained by scaling the $r_s = 1$ orbital. The kinetic energy scales as r_s^{-2} . To enable us to plot all values of r_s on the same plot, we rescale both axes and plot the fractional DMC truncation error, defined as $\text{Error}(R_{cut}) = [E(R_{cut}) - E_\infty]/E_\infty$ as a function of R_{cut}/r_s . After this rescaling the convergence plots for each value of r_s fall on a similar curve. Note, the negative truncation error around $R_{cut}/r_s = 6$ resulting from a loss of kinetic energy, due to abrupt truncation of the orbitals. This curve shows that the total DMC energy is approximately converged for truncation radii of $7 - 8r_s$. These converged values are in excellent agreement with the original values from Ceperley and Alder[19]. Therefore, while the slower polynomial decay of the density matrix of metallic systems requires a larger truncation radius to converge the total energy than for semiconductors with equivalent density, the above procedure for generating non-orthogonal orbitals does allow the localized orbitals for metallic systems to be truncated in a practical volume for linear scaling calculations. In addition, the above procedure for generating these non-orthogonal orbitals does not require the high symmetry of the HEG and therefore this approach could be equally applied to linear scaling DMC calculations of realistic metallic systems.

In conclusion, we derive a simple, automatic preprocessing procedure for generating non-orthogonal localized orbitals which minimize the total computational cost of linear scaling QMC calculations. We demonstrate the application of these orbitals to DMC calculations of the prototypical semiconductor and metallic systems, silicon and the HEG. We anticipate that these orbitals may also have applications in alternative electronic structure techniques such as DFT which also utilize localized orbitals to generate linear scaling.

The authors would like acknowledge G. Galli, R. Needs, R. Hood and D. Prendergast for helpful discussions and comments. This work was performed under the auspices of the U.S. Department of Energy by the University of California, Lawrence Livermore National Laboratory under contract No. W-7405-Eng-48.

* Electronic address: reboredo1@llnl.gov

[†] Electronic address: williamson10@llnl.gov

- [1] G. Galli, Phys. Stat. Sol. B **217**, 231 (2000).
- [2] X.P. Li, R.W. Nunes, and D. Vanderbilt, Phys. Rev. B **47**, 10891 (1993).
- [3] F. Mauri and G. Galli, Phys. Rev. B **50**, 4316 (1994).
- [4] J. Kim, F. Mauri, and G. Galli, Phys. Rev. B **52**, 1640 (1995).
- [5] E. Hernandez and M.J. Gillan, Phys. Rev. B **51**, 10157 (1995).
- [6] S. Liu, J. Perez-Jorda, and W. Yang, J. Chem. Phys. **112**, 1634 (2000).
- [7] M. Schutz, J. Chem. Phys. **114**, 661 (2001).
- [8] A.J. Williamson, R.Q. Hood, and J.C. Grossman, Phys. Rev. Lett **87**, 246406 (2001).
- [9] D. Alfe and M. Gillan, cond-mat/0404578 (2004).
- [10] N. Marzari and D. Vanderbilt, Phys. Rev. B **56**, 12847 (1997).
- [11] L. He and D. Vanderbilt, Phys. Rev. Lett. **86**, 5341 (2001).
- [12] I. Souza, N. Marzari, and D. Vanderbilt, Phys. Rev. B **65**, 035109 (2001).
- [13] A.J. Williamson, J.C. Grossman, R.Q. Hood, A. Puzder, and G. Galli, Phys. Rev. Lett. **89**, 196803 (2002).
- [14] A. Puzder, A.J. Williamson, F.A. Reboredo, and G. Galli, Phys. Rev. Lett. **91**, 157405 (2003).
- [15] R. Needs, G. Rajagopal, M. Towler, P. Kent, and A. Williamson, *CASINO code, version 1.6 User's Manual*, University of Cambridge (2002).
- [16] W. Foulkes, L. Mitas, R. Needs, and G. Rajagopal, Rev. Mod. Phys. **73**, 33 (2001).
- [17] Adjusting R_{cut} introduces minimal cost for QMC calculations as the radii are adjusted once before the calculation.
- [18] F.Gygi, *The GP Code*, LLNL (2004).
- [19] D.M. Ceperley and B.J. Alder, Phys. Rev. Lett. **45**, 566 (1980).